11th International Conference on Fracture Mechanics of Concrete and Concrete Structures
FraMCoS-11
J. M. Chandra Kishen, A. Ramaswamy, S. Ray and R. Vidyasagar (Eds)
https://doi.org/10.21012/FC11.092314

MODELLING THE BEHAVIOR OF RC BEAMS SIMULTANEOUSLY STRENGTHENED FOR FLEXURAL AND SHEAR WITH CFRP SYSTEMS

PEDRAM AYYOBI [*], JOAQUIM A. O. BARROS [†] AND SALVADOR J. E. DIAS [††]

[*] *Researcher, University of Minho, ISISE, ARISE, Dep. Civil Engineering*
Guimarães, Portugal
e-mail: pedram.ayyobi@gmail.com

[†] *Full Professor, University of Minho, ISISE, ARISE, Dep. Civil Engineering*
Guimarães, Portugal
e-mail: barros@civil.uminho.pt

[††] *Assistant Professor, University of Minho, ISISE, ARISE, Dep. Civil Engineering*
Guimarães, Portugal
e-mail: sdias@civil.uminho.pt

Key words: Numerical simulations, Carbon fiber reinforced polymers, Externally bonded reinforcement, Premature debonding, Near Surface Mounted

Abstract: By performing an experimental program, the performance of a hybrid solution using carbon fiber reinforced polymer (CFRP) systems for the simultaneous flexural and shear strengthening of T-cross section RC beams is assessed. In this solution, CFRP laminates are applied according to the near surface mounted technique for the flexural strengthening, while U-shape CFRP discrete strips of wet lay-up sheet are applied according to the externally bonded reinforcement technique for the shear strengthening. Furthermore, an innovative anchorage system using CFRP was developed for increasing the shear strengthening effectiveness of the abovementioned strips of CFRP sheets (avoiding premature debonding). To obtain extra information for assisting on the interpretation of the contribution of the CFRP anchorages on the performance of the hybrid CFRP solution, numerical simulations were carried out, by considering the nonlinear behavior of the concrete and steel reinforcements, and the CFRP-concrete bond conditions. This paper summarizes the relevant aspects of the experimental program, and details the numerical simulations.

1 INTRODUCTION

The use of Carbon Fiber Reinforced Polymer (CFRP) materials offers several benefits for strengthening reinforced concrete (RC) beams. Two main CFRP strengthening techniques, Near Surface Mounted (NSM) and Externally Bonded Reinforcement (EBR), are widely employed. CFRP materials provide advantages such as high strength-to-weight ratio, durability, easy and fast application [1]–[4].

The NSM technique has been found to be more efficient than the EBR for strengthening RC beams, considering strengthening increase, CFRP applied and time of execution. The effectiveness of NSM is influenced by parameters such as dimensions and distance of grooves, concrete quality of the substrate, geometry and surface treatment of the CFRP reinforcements, and properties of the adhesive [5]–[10]. However, premature rip-off failure

mode occurring in beams flexurally strengthened with NSM-CFRP reinforcements avoids to exploit integrally the strengthening potential of these reinforcements [11], [12].

In some cases, the flexural strengthening of some RC beams also requires shear strengthening intervention due to insufficient existing steel stirrups. In these cases, wet layup strips of CFRP of U configuration, applied according to the EBR technique, are used for providing the required shear strengthening [13]-[16]. By involving the NSM-CFRP reinforcements, these U-shape CFRP strips can simultaneously ensure the required shear resistance and avoid the occurrence of premature rip-off failure mode [17].

The shear strengthening efficiency of U shape CFRP strips is compromised by their premature debonding. To avoid this premature failure mode, several anchorage types are being proposed [18], [19]. Recently, Dias et al. [5] proposed a hybrid solution using NSM-EBR technique for shear and flexural behavior. The technique uses U shaped EBR CFRPs with ⋂ shaped anchorage for shear and NSM laminates for flexural strengthening. The anchorage prevents early debonding of EBR and improves the shear behavior of the beam.

The experimental program is limited in its ability to evaluate all aspects of the novel strengthening technique due to the large number of parameters involved. However, advanced finite element simulation software can provide a cost-effective and efficient solution to this issue. This study focuses on numerically simulating three types of beams tested in [5], by using a software capable of simulating the relevant nonlinear features of the intervenient materials. The simulation aims to predict the behavior of the beams in terms of load-displacement, crack pattern, strain in CFRP reinforcements, and debonding of EBR technique.

2 EXPERIMENTAL PROGRAM

2.1 Tested beams and materials properties

This section provides the fundamental information of a series of three RC beams of the experimental program described in detailed elsewhere [5]. Figure 1 illustrates the geometric dimensions, reinforcement details, loading and support conditions of the tested beams, to be numerically simulated.

In these three beams, three bars of 20 mm diameter ($3\phi 20$) were adopted for the longitudinal tensile steel reinforcements, while steel stirrups of 6 mm diameter spaced at 300 mm (ϕ6@300mm) were used as transverse reinforcement. Six bars of 12 mm diameter ($6\phi 12$) were used as longitudinal steel reinforcement in the flange for all beams.

A three-point loading scheme with different lengths of the beam shear spans was used in order the shear failure occur on the shortest shear span. The ratio of the beam span (a) to the effective depth of the beam (d_s) is 2.5, since it promotes the occurrence of shear tension failure mode [20], [21].

To prevent brittle spalling of the cover concrete at the beam supports, a two-directional cage of horizontal steel bars of 6 mm diameter at 65 mm spacing and vertical steel bars of 10 mm diameter at 50 mm spacing was applied in the zones indicated as "confined zone" of Figures 1a, 1c, 1e and 1h.

The two strengthened beams (**SFS-I and SFSA-I beams**) are equal to the reference beam (**REF-I** beam that is shown in Figure 1a and 1b), apart the following aspects:

SFS-I (Figure 1c and 1d) and **SFSA-I** (Figure 1e and 1f): these beams were flexurally strengthened using four CFRP laminates, with 1.4×10 mm^2 of cross section and spaced at 36 mm, applied according to the NSM technique (Figures 1d, 1f and 1g). They were also shear strengthened with U-shape CFRP discrete strips of wet lay-up sheet (two layers per strip, each one of 0.176 mm thickness) applied according to the EBR technique.

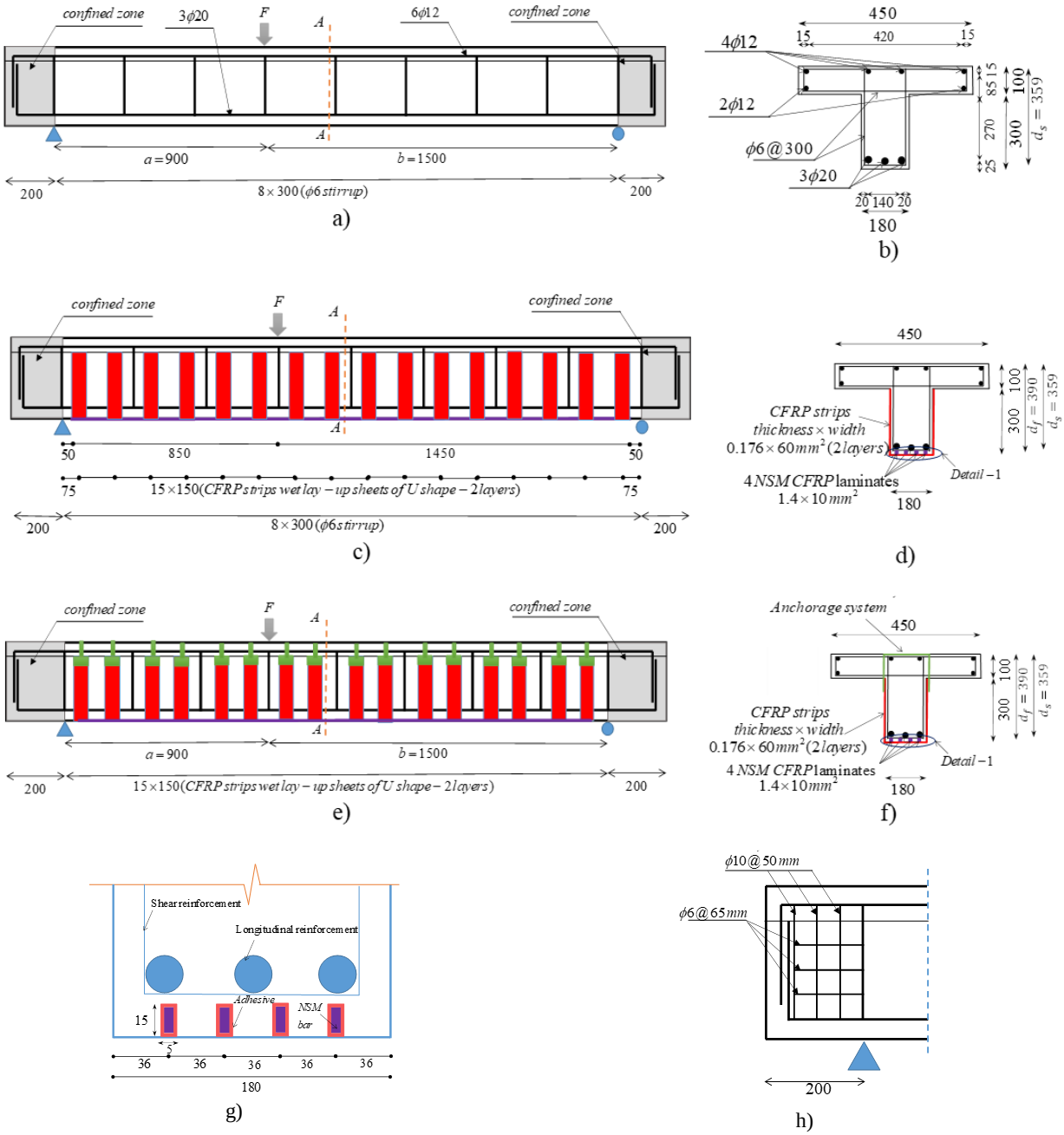

Figure 1: Series I of the experimental test [5] (dimensions in mm): a) reference beam (REF-I), b) section A-A of REF-I, c) strengthened beam without anchorages (SFS-I), d) section A-A of SFS-I, e) strengthened beam with anchorages (SFSA-I), f) section A-A of SFSA-I, g) detail-1, h) confined zone detail.

SFSA-I (Figure 1e and 1f): The unique difference of this beam regarding the **SFS-I** is the anchorage system provided in the top part of each layer of the U-CFRP strips in an attempt of offering resistance to their premature debonding from this region that would decrease their shear strengthening efficiency [5], [22]. The anchorage system consisted of an inverted U-shaped CFRP strip (⋂) and is divided in two parts: the rolled part in the flange and the overlap part (in the lateral faces of the beams´ web). In this last part, it was guaranteed per face the bond area that was determined experimentally (40×50 = 2000 mm^2) to ensure sufficient bonding area between the extremities of U and ⋂ shaped strips [5].

The flexural and shear reinforcement and strengthening ratios of the beams are indicated in Table 1.

Table 1: Details of the tested beams.

Beam	ρ_{sl} [1] (%)	CFRP flexural strengthening		ρ_{sw} [3] (%)	CFRP shear strengthening		
		Technique	ρ_{fl} [2] (%)		Technique	ρ_{fw} [4] (%)	Anchorage
REF-I	1.46	-	-	0.1	-	-	-
SFS-I	1.46	NSM	0.08	0.1	EBR	0.16	No
SFSA-I	1.46	NSM	0.08	0.1	EBR	0.16	Yes

[1]Flexural steel reinforcement percentage, $\rho_{sl} = A_{sl} \times 100 / b_w d_s$, where A_{sl} is the cross sectional area of the bottom steel bars, b_w is width of the beam's web and d_s is the internal arm of this reinforcement (Fig. 1b).

[2]Flexural CFRP strengthening percentage, $\rho_{fl} A = _f \times 100 / b_w \times d_f$, where A_f is the cross sectional area of NSM laminates and d_f is the internal arm of this reinforcement (Fig. 1d and 1f).

[3]Shear steel reinforcement percentage , $\rho_{sw} = A_{sw} \times 100 / b_w s_w$, where A_{sw} is cross sectional area of the two legs forming a steel stirrup, and s_w is the spacing of stirrups (Fig. 1a and 1b).

[4]Shear CFRP strengthening percentage, $\rho_{wf} = (2 \times t_f \times n_f \times b_f) \times 100 / (b_w \times s_f \times \sin\theta_f)$, where t_f, n_f, b_f and s_f are the thickness, the number of layers (=2), the width and the spacing of CFRP wet lay-up strip, respectively, while θ_f is the angle between the direction of the CFRP fibers and the beam's axis (Figure 1c to 1f).

The mean values of the material properties are presented in Table 2, namely: the mean cylindrical compressive strength (f_{cm}) and modulus of elasticity (E_{cm}) of concrete at the age when the beams were tested; the mean yield stress (f_{sym}) and ultimate tensile strength (f_{sum}) of steel reinforcements; and the mean tensile strength (f_{fum}), modulus of elasticity (E_{fm}) and maximum strain of CFRP laminates and CFRP sheets.

2.2 Strengthening procedures

The beams were flexurally strengthened with NSM CFRP laminates and shear strengthening with EBR U-shape CFRP discrete strips of wet lay-up sheet. The process involved opening grooves on the tension side of the beams, cleaning the grooves and laminates, and applying S&P Resin 220 epoxy adhesive for bonding the CFRP laminates to the concrete substrate into the grooves. The laminates were inserted into the grooves and adhesive in excess was removed. For the shear strengthening, the surface cement paste of the concrete substrate was removed, and the edges of the beams were rounded. In the SFSA-I beam, with a CFRP anchorage system, holes with 10 mm of diameter were drilled in its flange. EBR CFRP strips (2 layers) were installed using S&P Resin 55 epoxy adhesive (SFS-I and SFSA-I). In the beam SFSA-I the anchorage was executed after the application of each layer of the U-shape strip. The S&P Resin 55 epoxy adhesive was used to bond the CFRP anchorages to the concrete substrate. Details on the strengthening procedures can be consulted elsewhere [5].

Table 2: Material properties.

Concrete (at age of beams' tests)	f_{cm} (MPa)	E_{cm} (GPa)	
	44.3	34.1	
Steel	Diameter (mm)	f_{sym} (MPa)	f_{sum} (MPa)
	ϕ6	641	737
	ϕ20	636	767
CFRP laminate	f_{fum} (MPa)	E_{fm} (GPa)	ε_{fu} (‰)
	3165	175	18.0
CFRP sheet	f_{fum} (MPa)	E_{fm} (GPa)	ε_{fu} (‰)
	3096	245	12.6

2.3 Monitoring system

The experimental tests were carried out in a three-point loading configuration (Figure 2), with a servo-hydraulic closed-loop control equipment of 600 kN capacity, disposing a load cell of 500 kN capacity. The signal was read in a Linear Variable Differential Transformer (LVDT), installed in the loaded section, to control the test at a displacement rate of 0.01 mm/sec. LVDT_1 to LVDT_5, supported on an aluminum bar fixed on the beam over its supports to exclude the registration of parasitic displacements, were used to measure the beam's deflection (Figure 2).

Figure 3 shows the strain gauges installed in the CFRP of the beams SFS-I and SFSA-I. For the flexural strengthening system (NSM laminates), two strain gauges were installed (SG_CL1 and SG_CL2), one at the loaded section and the other at the middle of the shear span. Two strain gauges were bonded in each of the two CFRP strips considered to have the highest probability of contributing to the beam's shear strengthening (SG_CV1 to SG_CV4). During each test, the cracking process was registered in one of the lateral faces of the beam, by indicating the load level to the corresponding crack pattern.

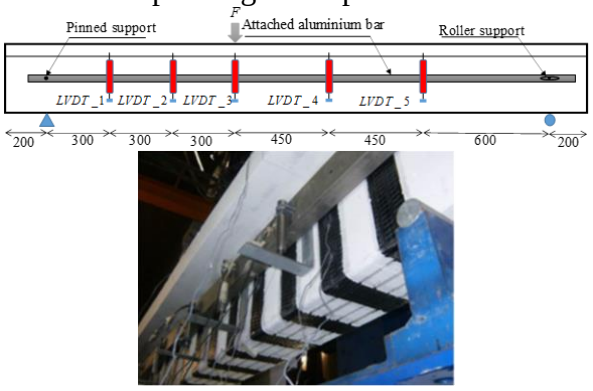

Figure 2: Disposition of the LVDTs for measuring the beam's deflection (dimensions in mm): a) schematic representation, b) photo [5].

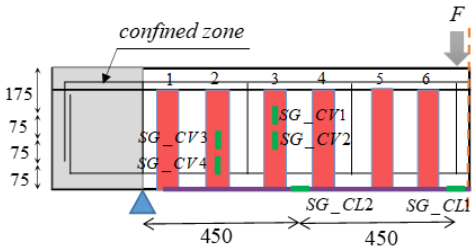

Figure 3: Disposition of the strain gauges in the NSM laminates (SG-CL1 and SG-CL2) and EBR U-CFRP (SG_CV1, SG_CV2, SG_CV3 and SG_CV4) of SFS-I and SFSA-I beams (dimensions in mm) [5].

2.4 Relevant experimental results

Table 3 presents the maximum load supported by the beam, F_{max}, its deflection at loaded section, u_{LS}, failure mode, and maximum strains recorded by strain gauges in the NSM CFRP laminates and U-CFRP strips. The recorded experimental results are graphically presented in the section of the numerical simulations of the tested beams, when assessing the predictive performance of the adopted numerical model.

The strengthened RC beam with the hybrid CFRP configuration and shear strengthening anchorage system (SFSA-I) showed a substantial increase in load carrying capacity. This beam, failed by flexural, exhibited a maximum load that was 54% higher than the reference beam without CFRP and 31% higher than the strengthened RC beam without the shear strengthening anchorage system. Furthermore, the SFSA-I beam showed a 128% increase in deflection at maximum load compared to the reference beam without CFRP and a 174% increase compared to the strengthened RC beam without the shear strengthening anchorage system.

Table 3: Main experimental results.

Beam	F_{max} (kN)	u_{LS} (mm)	Failure mode	Maximum strains (‰)					
				CL1	CL2	CV1	CV2	CV3	CV4
REF-I	310.3	12.54	shear	-	-	-	-	-	-
SFS-I	365.1	10.44	shear	-	3.7	3.0	2.1	4.3	4.4
SFSA-I	479.0	28.59	flexural	12.1	3.6	4.7	2.2	4.6	4.2

.

3 NUMERICAL SIMULATIONS

3.1 Brief description of the CDP and material constitutive laws

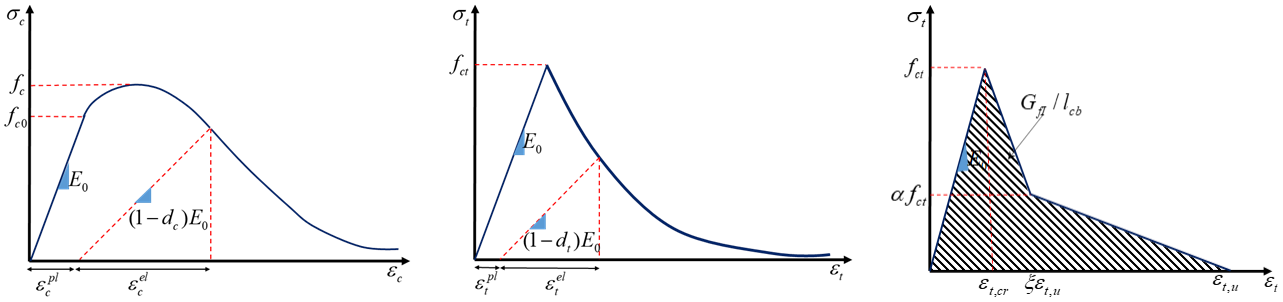

Figure 4: Concrete uniaxial behaviour in: a) compression, and b) tension; c) tensile diagram adopted in the numerical simulations [23].

According to the Concrete Damage Plasticity (CDP), the tensile and compressive concrete behavior is simulated by the following stress-strain equations (Figure 4) [23]:

$$\sigma_t = (1-d_t)E_0(\varepsilon_t - \varepsilon_t^{pl}) \quad (1)$$

$$\sigma_c = (1-d_c)E_0(\varepsilon_c - \varepsilon_c^{pl}) \quad (2)$$

where σ_t and ε_t are the tensile stress and strain, σ_c and ε_c are the compressive stress and strain and E_0 is the concrete longitudinal modulus of elasticity. In these equations, d_t and d_c are the damage parameters in tension and compression, respectively, varying between 0 to 1 (undamaged to totally damaged concrete) to simulate the loss of stiffness with the increase of the corresponding concrete plastic strain in tension and compression (ε_t^{pl} and ε_c^{pl}), determined from:

$$\varepsilon_t^{pl} = \varepsilon_t - \frac{d_t}{(1-d_t)}\frac{f_{ct}}{E_0} \quad (3)$$

$$\varepsilon_c^{pl} = \varepsilon_c - \frac{d_c}{(1-d_c)}\frac{f_{c0}}{E_0} \quad (4)$$

with f_{ct} and f_{c0} being the concrete tensile strength, and the concrete compressive stress above which the behavior in compression becomes nonlinear (Figure 4). The concrete compressive behavior is simulated according to Mander's model [24].

Modeling the uniaxial tension behavior

The concrete post-cracking tensile behavior is simulated by the diagram represented in Figure 4c, where mode I fracture energy, G_{fl}, the f_{ct} and the bilinear shape were determined according to the recommendations of Model Code 2010 [25], with small adjustments. In an attempt of having results not dependent on the refinement of the finite element mesh, the area behind the tensile stress-strain diagram is considered the G_{fl}/l_{cb}, where l_{cb} is the crack bandwidth, admitted equal to the edge of the almost cubic shape of the adopted solid finite elements (Figure 4c). This means that different l_{cb} values were adopted in the simulations with different mesh refinement.

Modeling the concrete multiaxial behavior

The multiaxial stress-strain relationship of concrete is simulated from:

$$\sigma = (1-d)D_0^{el} : \left(\varepsilon - \varepsilon^{pl}\right) \quad (5)$$

where D_0^{el}, σ and ε are the elastic stiffness (that depends on the modulus of elasticity and Poisson coefficient of concrete), stress and strain tensors, respectively, while d is a scalar damage parameter representing the damage in tension and compression. To determine the evolution of the stress field and the plastic strains, attending the concrete

resistance under multiaxial stress field, the following yield surface function is adopted:

$$F=\frac{1}{1-\alpha}(q-3\alpha p+\beta\langle\sigma_{\max}\rangle-\gamma -\langle\sigma_{\max}\rangle)-\bar{\sigma}_c=0 \quad (6)$$

where,

$$0\le\alpha=\frac{(f_{b0}/f_{c0})-1}{2(f_{b0}/f_{c0})-1}\le 0.5 \quad (7)$$

$$\beta=\frac{\bar{\sigma}_c(\varepsilon_c^{pl})}{\bar{\sigma}_t(\varepsilon_t^{pl})}(1-\alpha)-(1+\alpha) \quad (8)$$

$$\gamma=\frac{3(1-K_c)}{2K_c-1} \quad (9)$$

In Eq. (6) $\langle.\rangle$ is the Macaulay bracket ($\langle x\rangle=1/2(|x|+x)$), $p=-1/3\sigma:I$ is the hydrostatic equivalent pressure, $q=\sqrt{2/3S:S}$ is the Von Mises equivalent deviatoric stress (with $S=pI+\sigma$), and $\sigma_{\max}$ is the maximum principal effective stress. In Eq. (7) f_{b0} is the concrete biaxial yield strength in compression, In Eq. (8) $\bar{\sigma}_c$ and $\bar{\sigma}_t$ are the equivalent stress in compression and tension, respectively. Finally, K_c is a parameter ranging between 0.5 and 1.0, being generally adopted equal to 2/3 for concrete.

For considering the nonlinear volume change of concrete in compression, the CDP adopts a non-associated flow rule based on the following flow potential function:

$$G=\sqrt{(ef_{ct}\tan\psi)^2+q^2}-p\tan\psi \quad (10)$$

where ψ is the dilation angle measured in the *p vs q* relationship, and e is a parameter that defines the rate at which the *G* function approaches the asymptote (Figure 5, where ϕ is the concrete internal friction angle).

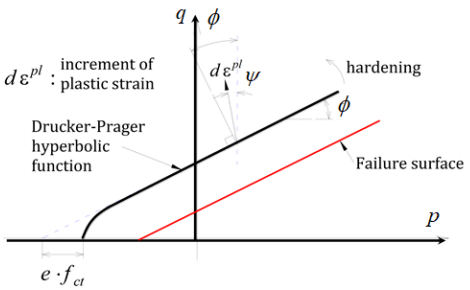

Figure 5: Non-associated potential function considered in CDP [23].

Modeling the contact between concrete and CFRP strips

The NSM-CFRP laminates were considered perfectly bonded to the substrate. However, for the EBR-CFRP strips of wet lay-up sheets debonding was possible to occur, which was simulated by the following failure criteria:

$$\max\left\{\frac{\langle t_n\rangle}{t_n^0},\frac{t_s}{t_s^0},\frac{t_t}{t_t^0}\right\}=1 \quad (11)$$

where t_n^0, t_s^0 and t_t^0 is the resisting tensile and shear strength of the adhesive (the shear strength was assumed equal in the two shear directions, s and t). To simulate the sliding components, it was considered the τ_b-s relationship proposed in fib bulletin 90 [26], represented in Figure 6, therefore $t_s^0=t_t^0=\tau_{b1}$.

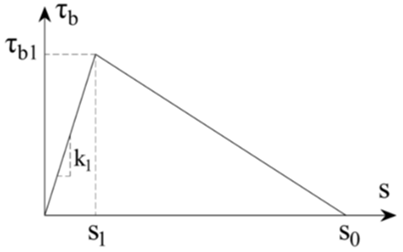

Figure 6: Constitutive law for bond in EBR FRP system [26].

The stress filed in this contact is determined from the following equations:

$$t_{nd}=\begin{cases}(1-D)t_n^0, t_n^0\ge 0\\ t_n^0, t_n^0\le 0\end{cases} \quad (12)$$

$$t_{sd}=(1-D)t_s^0 \quad (13)$$

$$t_{td}=(1-D)t_t^0 \quad (14)$$

where D is a scalar damage parameter ranging from 0 to 1, determined from:

$$D=\frac{s_0(s_m^{\max}-s_1)}{s_m^{\max}(s_0-s_1)} \quad (15)$$

being s_1 and s_0 the slip at peak bond strength and ultimate slip, whose values are those proposed by fib Bulletin 90, while $s_m^{\max}$ is the maximum slip between the two sliding directions, s_s and s_t, respectively, i.e., $s_m^{\max}=\max(s_s;s_t)$.

3.2 Finite element mesh, support and loading conditions, and values of the model's parameters

Due to the theoretical longitudinal symmetry of the testing beam conditions, only half of the beam was simulated. The boundary and supported conditions and steel bar reinforcements are represented in Figure 7. The adopted values of CDP model are indicated in Table 4.

The concrete part was modelled with eight-node solid finite elements (C3D8) with Gauss-Legendre integration scheme of 2×2×2. The steel reinforcement was modelled with 2-node 3D truss element (T3D2), considered perfectly bonded to the surrounding concrete (Figure 10). The NSM laminates were modelled with 2-node beam element (B31) of 50 mm size. The CFRP strips were modelled with a type of finite element that only considers the membrane stiffness (4-node quadrilateral, M3D4), of 35 mm edge size [23].

Table 4: Values of the CDP model parameters adopted in the numerical simulations.

Parameters	Adopted values
Dilation angle, ψ (Degree)	40
e	0.1
f_{b0}/f_{c0}	1.16
K_c	0.667
f_{ct} (MPa)	2.1
G_{ft}(N.m)	100
α	0.2
ξ	0.05
Crack band width:	
Mesh 30mm	30 mm
Mesh 35mm	35 mm
Mesh 50mm	50 mm
f_l/f_c^* (REF-1 and SFS-1)[26]	0.0
f_l/f_c((SFSA-I)[26]	0.26
f_c (MPa)	44.3
E_0(GPa)	27.28
ε_{cu}	0.0045

*Confinement level according to [24].

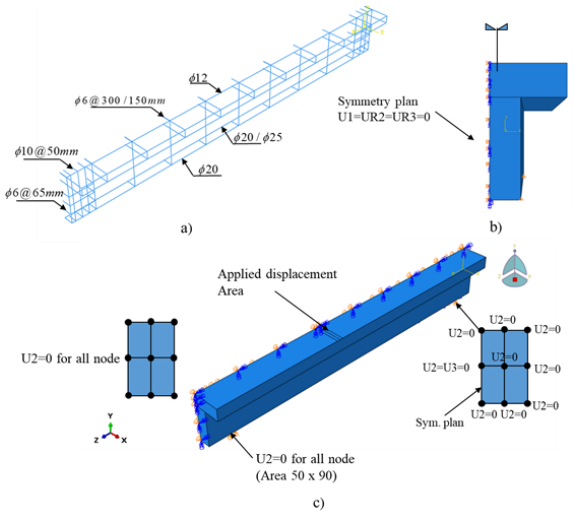

Figure 7: Boundary and support conditions.

4 NUMERICAL RESULTS

3.1 Influence of FE mesh refinement

A sensitivity analysis was conducted on the influence of the refinement of the finite element (FE) mesh on the force *vs* loaded-section deflection. For this purpose, the reference beam REF-I, was considered, and the results are presented in Figure 8. It is verified a tendency for a decrease of the load carrying capacity with the decrease of the size of the FE. The compromise in terms of accuracy and computing time suggests a mesh size of 35 mm, which will be the mesh refinement of the hereafter simulations (Figure 9). Figure 14a shows the crack pattern predicted numerically (with the Mesh=35mm) and observed experimentally, demonstrating the model was capable of localizing the occurrence of the critical diagonal crack.

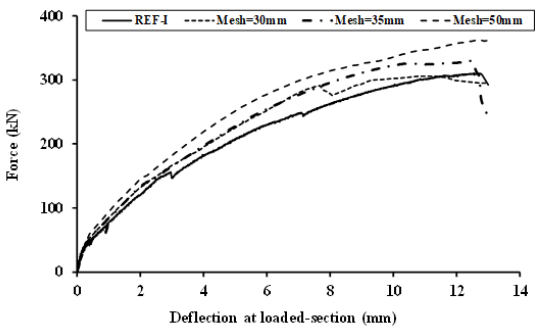

Figure 8: Sensitivity analysis in terms of the refinement of the finite element mesh.

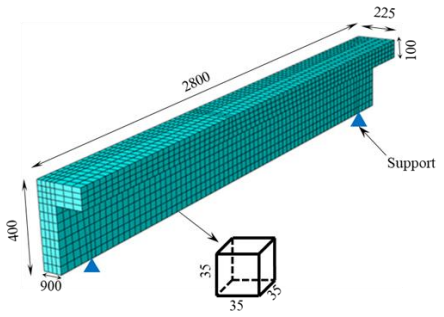

Figure 9: Mesh size of the reference beam (35 mm).

4.2 Influence of bond conditions in the U-shape EBR-CFRP strips

The influence of the bond conditions between U-shape EBR-CFRP strips and concrete substrate was investigated by simulating the load-deflection of the SFS-I beam. The following two bond conditions were considered: 1) perfect bond; 2) debonding according to *fib* bulletin 90 recommendations (Figure 6), adopting for the defining parameters the following values: τ_{b1}=6.95MPa, s_1=0.0107mm and s_0=0.24mm. Figure 10 compares the numerical simulation and experimental results. Above a deflection of about 6 mm, a significant decrease of stiffness was observed when assuming debonding, having been anticipated the failure of the beam. When perfect bond was considered, the degradation of stiffness was much smaller, and failure of the beam was not captured up to the maximum deflection registered experimentally.

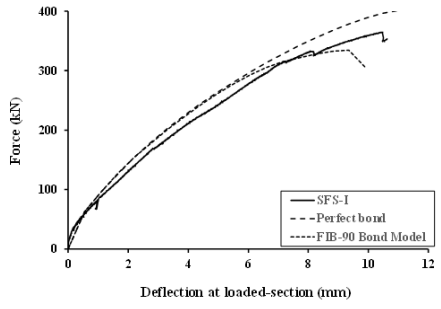

Figure 10: Comparison between experimental and numerical relationships of force versus deflection.

In the SFS-I beam, the failure mode occurred by debonding of the wet lay-up CFRP sheets that were intersected by the shear failure crack [5]. Figure 14b shows the crack pattern in the SFS-I beam in the eminence of failure. At about a deflection of 8.2 mm and load of 330 kN in the experimental test, the top part of the third CFRP strip from the beam's left support (strip 3) has debonded, conducting to a drop on the beam's load carrying capacity, with a progression of the shear failure crack towards the second CFRP strip (from beam's the left support - strip 2). The force supported by the strip 3 was transferred to the other shear ligaments, leading to an increment of the force supported by the beam, up to the moment when the top part of strip 2 has debonded, corresponding to the collapse of the beam.

By using the $\tau - s$ proposed by fib bulletin 90 (with τ_{b1}=6.95MPa, s_1=0.0107mm and s_0=0.24mm) the debonding of these two strips has initiated earlier than experimentally, resulting in a higher degradation of the beam's stiffness and an anticipation of their debonding (Figure 14b in top). By increasing the s_0 and τ_{b1} of the $\tau - s$ proposed by fib bulletin 90 to 0.3 mm and 8.5 MPa, respectively, Figure 11 shows that the premature debonding reported previously was not occurred, resulting in a significant increment on the beam's load carrying capacity, which shows its dependency on the properties attributed to the $\tau - s$.

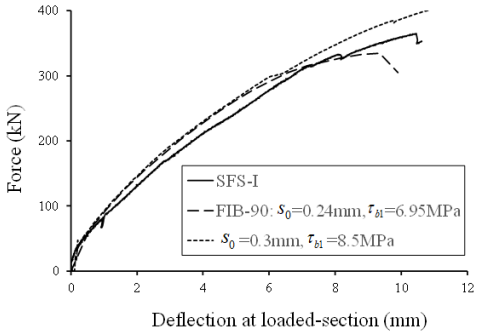

Figure 11: Influence of the values defining the *fib* bulletin 90 $\tau - s$ on the force-deflection of SFS-I.

Figure 12 compares the relationship between the strain in the SG-CV1 (Figure 3) and the applied load registered experimentally and predicted numerically for the different bond conditions of the CFRP strips already considered. It is verified that all numerical simulations predicted smaller strains than the

values recorded experimentally, with improvements when the possibility of sliding is considered in the simulations. The predictions become closer to the experimental strains during the loading process, being very close at the failure of the beam when $\tau - s$ proposed by fib bulletin 90 is used with the values of 0.3 mm and 8.5 MPa for the parameters s_0 and τ_{b1}, respectively. However, this tendency cannot be generalized, since the evolution of the strains in a certain strain gauge is quite dependent on its localization regarding the closest crack crossing the CFRP strip where it is installed. A recent blind simulation competition [27] demonstrated the models of continuous nature, like the one used in the present simulations, have worst predictive performance than discrete crack models in terms of strains in the constituent materials and crack width at serviceability limit state conditions.

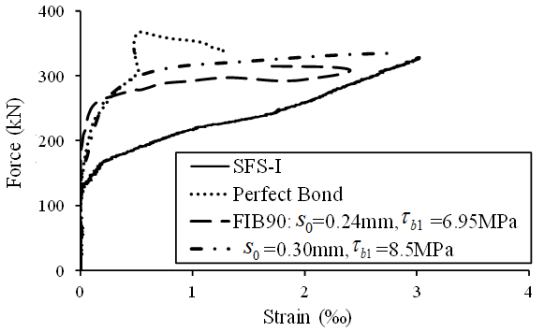

Figure 12: Experimental and numerical force *vs* strain in the SG-CV1 of SFS-I beam.

4.3 BEAM SFSA-I

Figure 13 compares the experimental to the numerical force versus deflection of SFSA-I beam (strengthened with anchorages). Perfect bond conditions were considered for the CFRP strips and anchorages. The numerical simulation has predicted a peak load 6% higher than the one registered experimentally. This was mainly caused by a little bit higher stiffness in the elasto-cracked stage in the numerical simulation, since the stiffness after yield initiation of the flexural reinforcement has a trend very close to the one observed experimentally. The longitudinal steel bars started to yield at 9.60 mm deflection and 390 kN force in the numerical simulation, and at 10.2 mm deflection and 393 kN force in the experiment. The numerical and experimental crack patterns at failure are represented in Figure 14c, where it is visible the model was able to predict a flexural failure mode.

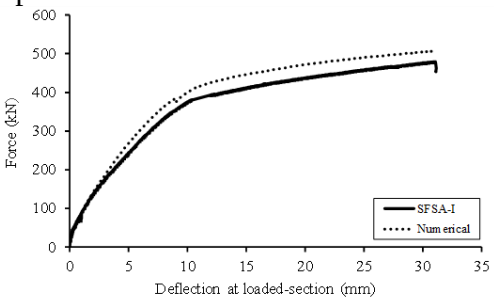

Figure 13: Experimental and numerical relationships of force versus deflection of SFSA-I beam.

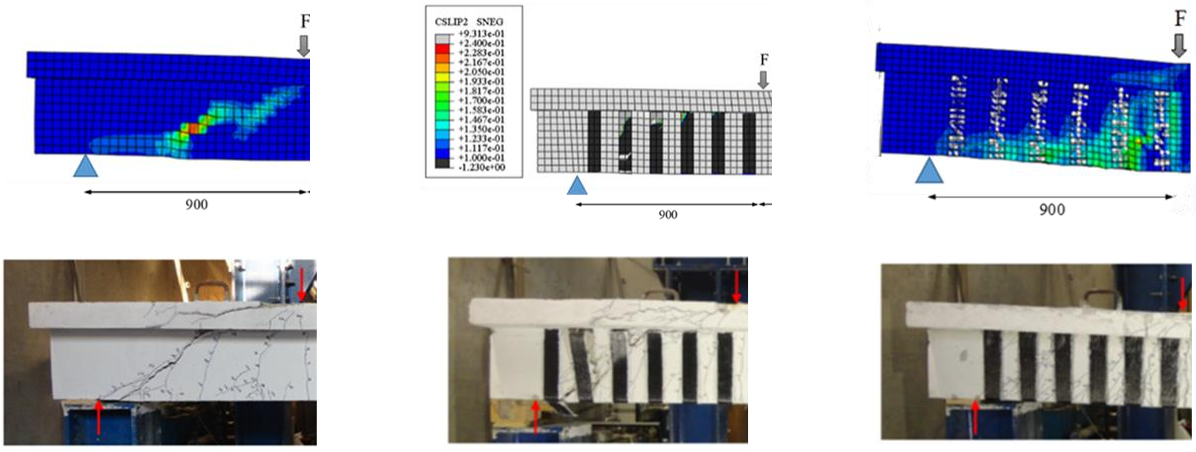

Figure 14: Crack pattern at failure of the beams: a) REF-I, b) SFS-I and c) SFSA-I.

CONCLUSIONS

This work presented an experimental program with almost real scale RC beams of T cross section, where an innovative CFRP anchorage was applied in an attempt of

increasing the shear capacity of this type of beams when shear strengthened with wet layup U shape CFRP strips. The anchorage demonstrated capable of transforming the brittle shear failure, observed in the beam exclusively shear strengthened with U shape CFRP strips, in a flexural failure model, with a significant increment on the beam's load carrying capacity and its ductility (deformational performance).

A critical analysis on the use of the CDP for modelling this type of beams was performed, by investigating the influence of the mesh refinement and bond conditions of the CFRP on the relevant results. From the analysis it was verified a tendency for a decrease of the load carrying capacity with the decrease of the size of the FE, but a mesh with finite elements of dimension less than 3 times the maximum dimension of the concrete aggregates provides acceptable level of predictive performance. Regarding the bond conditions of the wet layup U shape CFRP strips, it was verified that the bond law proposed by fib bulletin 90 anticipates the debonding process and the consequent failure of the strengthened beam, being the beam's load carrying capacity

significantly dependent on the values attributed to the parameters defining this bond law. However, even considering the perfect bond conditions for the U shape CFRP strips, the model could predict the failure modes observed experimentally on the strengthened beams.

ACKNOWLEDGEMENTS

This study is a part of the project "Sticker", with the reference POCI-01-0247-FEDER-039755. The first author acknowledges the research grant support provided by this project. This work was partly financed by FCT / MCTES through national funds (PIDDAC) under the R&D Unit Institute for Sustainability and Innovation in Structural Engineering (ISISE), under reference UIDB/04029/2020, and under the Associate Laboratory Advanced Production and Intelligent Systems ARISE under reference LA/P/0112/2020.

REFERENCES

[1] J.A.O. Barros, S.J.E. Dias, and J.L.T. Lima, "Efficacy of CFRP-based techniques for the flexural and shear strengthening of concrete beams", *Cem. Concr. Compos.*, vol. 29, no. 3, pp. 203–217, Mar.2007, doi: 10.1016 / j.cemconcomp. 2006.09.001.

[2] S.J.E. Dias and J.A.O. Barros, "Performance of reinforced concrete T beams strengthened in shear with NSM CFRP laminates", *Eng. Struct.*, vol. 32, no. 2, pp. 373–384, 2010, doi: 10.1016/j.engstruct.2009.10.001.

[3] C.E. Bakis *et al.*, "Fiber-Reinforced Polymer Composites for Construction - State-of-the-Art Review", *Perspect. Civ. Eng. Commem. 150th Anniv. Am. Soc. Civ. Eng.*, no. May, pp. 369–383, 2003, doi: 10.1061/(asce)1090-0268(2002)6:2(73).

[4] G. Muciaccia, M. Khorasani, and D. Mostofinejad, "Effect of different parameters on the performance of FRP anchors in combination with EBR-FRP strengthening systems: A review", *Construction and Building Materials*, vol. 354. Elsevier Ltd, Nov. 07, 2022.

[5] S.J.E. Dias, J.R.M. Silva, and J.A.O. Barros, "Flexural and shear strengthening of reinforced concrete beams with a hybrid CFRP solution", *Compos. Struct.*, vol. 256, no. September 2020, p. 113004, 2021, doi: 10.1016 / j.compstruct. 2020.113004.

[6] A. Bilotta, F. Ceroni, E. Nigro, and M. Pecce, "Efficiency of CFRP NSM strips and EBR plates for flexural strengthening of RC beams and loading pattern influence", *Compos. Struct.*, vol. 124, pp. 163-175, 2015, doi: 10.1016/ j.compstruct. 2014.12.046.

[7] W. Sun, T. Lou, and M. Achintha, "A novel strong and durable near-surface mounted (NSM) FRP method with cost-effective fillers", *Compos. Struct.*, vol. 255, p. 112952, 2021, doi: 10.1016/j.compstruct.2020.112952.

[8] Q. Wang, H. Zhu, T. Li, G. Wu, and X. Hu, "Bond performance of NSM FRP bars in concrete with an innovative additional ribs anchorage system: An experimental study", *Constr. Build. Mater.*, vol. 207, pp. 572–584, 2019, doi: 10.1016/j.conbuildmat.2019.02.020.

[9] A.M. Khalifa, "Flexural performance of RC beams strengthened with near surface mounted CFRP strips", *Alexandria Eng. J.*, vol. 55, no. 2, pp. 1497–1505, 2016, doi: 10.1016/j.aej.2016.01.033.

[10] I.A. Sharaky, L. Torres, J. Comas, and C. Barris, "Flexural response of reinforced concrete (RC) beams strengthened with near surface mounted (NSM) fibre reinforced polymer (FRP) bars", *Compos. Struct.*, vol. 109, no. 1, pp. 8–22, 2014, doi: 10.1016/j.compstruct.2013.10.051.

[11] M. Rezazadeh, J.A.O. Barros, and H. Ramezansefat, "End Concrete Cover Separation in RC Structures Strengthened in Flexure with NSM FRP: Analytical Design Approach", *Engineering Structures Journal*, 128, 415-427, December 2016. 10.1016/j.engstruct.2016.09.062.

[12] J.A.O. Barros and A.S. Fortes, "Flexural strengthening of concrete beams with CFRP laminates bonded into slits", *Cement and Concrete Composites*, vol. 27, pp. 471–480, 2005, doi: 10.1016/j.cemconcomp.2004.07.004.

[13] A. Mofidi, and O. Chaallal, "Shear strengthening of RC beams with externally bonded FRP composites: Effect of strip-width-to-strip-spacing ratio", *Journal of composites for construction*, 15(5), 732-742 (2011).

[14] M.K. Askar, A.F. Hassan, and Y.S.S. Al-Kamaki, "Flexural and shear strengthening of reinforced concrete beams using FRP composites: A state of the art", *Case Studies in Construction Materials*, 17, e01189, 2022.

[15] A.S. Karzad, M. Leblouba, S.A. Toubat, and M. Maalej, "Repair and strengthening of shear-deficient reinforced concrete beams using Carbon Fiber Reinforced Polymer", *Composite Structures*, 223, 110963, 2019.

[16] R. Kotynia, E. Oller, A. Marí, and M. Kaszubska, "Efficiency of shear strengthening of RC beams with externally bonded FRP materials – State-of-the-art in the experimental tests", *Composite Structures*, 267, 113891, 2021.

[17] J.A.O. Barros, I.G. Costa, and A. Ventura-Gouveia, "CFRP flexural and shear strengthening technique for RC beams: experimental and numerical research", *Advances in Structural Engineering Journal*, 14(3), 559-581, 2011.

[18] M.H. Arslan et al., "Shear strengthening of reinforced concrete T-beams with anchored and non-anchored CFRP fabrics," *Structures*, 39, 527–542, 2022, doi: 10.1016/j.istruc.2022.03.046.

[19] A. Mofidi et al., "Performance of End-Anchorage Systems for RC Beams Strengthened in Shear with Epoxy-Bonded FRP", *Journal of Composites for Construction*, 16(3), pp. 322–331, 2012.

[20] M.P. Collins and D. Mitchell, *Prestressed concrete structures*, vol. 9. Prentice Hall Englewood Cliffs, NJ, 1991.

[21] G.N.J. Kani, "The Riddle of Shear Failure and its Solution", *ACI J. Proc.*, vol. 61, no. 4, 1964, doi: 10.14359/7791.

[22] A. Eslami, A. Moghavem, H.R. Shayegh, and H.R. Ronagh, "Effect of FRP stitching anchors on ductile performance of shear-deficient RC beams retrofitted using FRP U-wraps", *Structures*, vol. 23, pp. 407–414, Feb. 2020, doi: 10.1016/j.istruc.2019.11.007.

[23] "ABAQUS, Documentation Version 2017: Hibbit, Karlson and Sorensen, Inc., USA."

[24] J.B. Mander, M.J.N. Priestley, and R. Park, "Conducted Providing the Stress-Strain Model for Confined Concrete", *J. Struct. Eng.*, vol. 114, no. 8, pp. 1804–1826, 1988.

[25] *fib* Model Code 2010: fib Model Code for Concrete Structures 2010.

[26] "Fib – Bulletin 90. Externally applied FRP reinforcement for concrete structures Technical report by Task Group 5.1 FRP (fiber reinforced polymer) reinforcement for concrete structures. Féderation Internationale du Béton – fib, May 2019. 240 pp."

[27] J.A.O. Barros et al., "Blind competition on the numerical simulation of continuous shallow steel-fibre reinforced concrete beams failing in bending", *fib Structural Concrete Journal*, 2023. https://doi.org/10.1002/suco.202200754.